Microstructured hydroxyl environments and Raman spectroscopy in selected basic transition-metal halides*

Liu Xiao-Dong(刘晓东)[a)b)†], Meng Dong-Dong(孟冬冬)[a)], Hagihala Masato(萩原雅人)[a)], and Zheng Xu-Guang(郑旭光)[a)c)]

[a)] *Department of Physics, Graduate School of Science and Engineering, Saga University, Saga* 840-8502, *Japan*

[b)] *Department of Physics, College of Science, Tianjin Polytechnic University, Tianjin* 300160, *China*

[c)] *Department of Physics, Faculty of Science and Engineering, Saga University, Saga* 840-8502, *Japan*

(Received 24 January 2011; revised manuscript received 14 February 2011)

Raman vibrational spectra of the selected basic (hydroxyl OH and deuteroxyl OD) transition-metal halides, geometrically frustrated material series α-, β-, γ-$Cu_2(OH)_3Cl$, α-$Cu_2(OH)_3Br$, β-$Ni_2(OH)_3Cl$, β-$Co_2(OH)_3Cl$, β-$Co_2(OH)_3Br$, γ-$Cu_2(OD)_3Cl$, and β-$Co_2(OD)_3Cl$ are measured at room temperature and analysed to investigate the relationship between the microstructured OH environments and their respective Raman spectra. Among these selected samples, the last two are used to determine the OH stretching vibration region (3600 cm^{-1}–3300 cm^{-1}) and OH bending vibration region (1000 cm^{-1}–600 cm^{-1}) of OH systems in the spectra. Through the comparative analysis of the distances d(metal–O), d(O–halogen), and d(OH), the strong metal–O interaction and trimeric hydrogen bond (C_{3v}, C_s or C_1 symmetry) are found in every material, but both determine simultaneously an ultimate d(OH), and therefore an OH stretching vibration frequency. According to the approximately linear relationship between the OH stretching vibration frequency and d(OH), some unavailable d(OH) are guessed and some doubtful d(OH) are suggested to be corrected. In addition, it is demonstrated in brief that the OH bending vibration frequency is also of importance to check the more detailed crystal microstructure relating to the OH group.

Keywords: hydroxyl, trimeric hydrogen bond, Raman spectrum, basic transition-metal halide

PACS: 78.30.–j, 33.20.Ea, 61.66.Fn, 61.12.–q **DOI:** 10.1088/1674-1056/20/8/087801

1. Introduction

The concept of the hydrogen bond (H-bond) is a century old but remains youthful because of its vital role in so many branches of science.[1−4] The H-bonds in solid hydroxides are especially attractive and are studied in the crossdisciplinary field that necessarily involves chemists, material scientists, crystallographers, and physicists.[5−14] Just about seven years ago our group was the first, to the best of our knowledge, to point out that seemingly simple inorganic coordination complex series, basic (hydroxyl OH and deuteroxyl OD) transition-metal halides $M_2(OH)_3X$ (M=Mn, Fe, Co, Ni, Cu; X=Cl, Br, I), possess the famous magnetic geometrical frustration properties,[15−30] many of which are not well understood till now.[23,29] Therefore, more and more teams have devoted effort to investigating them by more and more methods.[31−37] From the viewpoints of chemists and spectroscoptists, H-bonds must exist in this material series, which can be studied by the spectroscopic methods. To the best of our knowledge, the infrared (IR) and Raman spectra of four isomers of $Cu_2(OH)_3Cl$ were only reported by the Frost group from the mineralogical aspect.[38−40] This situation may result from the limitations of the sample preparation. Based on the study of spin–lattice coupling in the magnetic community, the optical spectroscopy of the magnetic geometrically frustrated materials is required to help understand the exotic properties at low transition temperatures by checking the lattice and bonding changes.[41,42] Because almost all lattice and bonding changes can lead to a position shift of the characteristic spectral bands or peaks, H-bonds and the OH distances must apparently be affected if the lattice and bonding changes are remarkable, and

*Project supported by the Grant-in-Aid for Scientific Research on Priority Area from the Ministry of Education, Culture, Sports, Science and Technology, Japan (Grant No. Tokutei 22014008).

†Corresponding author. E-mail: zjcxdl@163.com

© 2011 Chinese Physical Society and IOP Publishing Ltd

therefore the optical spectral data can give much very useful information. Those of the H-bond related OH systems are especially welcome because the fundamental mode frequencies of OH stretching vibration ν(OH) and bending vibration δ(OH) are more sensitive to the position change of its adjacent ions than other vibrational groups.

In this paper, Raman vibrational spectra of the selected basic (hydroxyl OH and deuteroxyl OD) transition-metal halides, geometrically frustrated material series α-, β-, γ-$Cu_2(OH)_3Cl$, α-$Cu_2(OH)_3Br$, β-$Ni_2(OH)_3Cl$, β-$Co_2(OH)_3Cl$, β-$Co_2(OH)_3Br$, γ-$Cu_2(OD)_3Cl$, β-$Co_2(OD)_3Cl$, are reported at room temperature and analysed to investigate the relationship between the microstructured OH environments and their respective Raman spectra. In addition to the H-bond in these samples, we also focus on the joint effect of adjacent metal ions on ν(OH) and δ(OH).

2. Materials and methods

2.1. Sample preparation

Except for the β-$Cu_2(OH)_3Cl$ (natural Atacamite from Arizona, USA), all other samples were prepared by hydrothermal reaction, and verified to be highly single phase by crystal structure measurements, see Refs. [15]–[29]. For example, the synthetic polycrystalline γ-$Cu_2(OH)_3Cl$ was prepared by using a solution reaction from 100 g of $Cu(HCOO)_2{\cdot}4H_2O$ and 40 g of KCl in purified water at 95 °C. The polycrystalline precipitate was thoroughly washed and filtered. The crystalline nature was further improved by a hydrothermal treatment at 200 °C for several hours.[17]

2.2. Crystal structure measurement

The crystal structures of samples were determined using synchrotron X-ray diffraction at beam line BL02B2, Spring-8 (Japan) and neutron powder scattering measurements conducted at HERMES, JAERI using a wave length of 1.8265 Å (1 Å=0.1 nm) or 1.4143 Å.[17−30]

2.3. Micro-Raman spectroscopy

Raman spectra were obtained using an HR800 HORIBA Jobin Yvon laser micro-Raman microscopy equipped with 10×, 50× and 100× objectives. Raman spectra were excited by a spectra-physics model 127 Ar^+ laser (488.0 nm) at a resolution of 0.5 cm^{-1} between 95 cm^{-1} and 4000 cm^{-1}. Repeated acquisitions using the highest magnification were accumulated to improve the signal-to-noise ratio in the spectra. Because the samples will be broken down to other chemicals at an intensive laser power density, 100× objective are used at laser powers of 5 mW–30 mW to obtain Raman signals strong enough. All Raman shift spectra are automatically baseline corrected, smoothed and normalized according to the largest counting peak value.

3. Results and discussion

3.1. Microstructure of the hydroxyl system

Both the synchrotron X-ray diffraction and neutron powder scattering measurements gave consistent results about their crystal structures and crystal parameters except the protons' positions. The space group numbers are as follows: α-$Cu_2(OH)_3Cl$ and α-$Cu_2(OH)_3Br$ belong to No. 11 (C_{2h}^2), β-$Cu_2(OH)_3Cl$ (natural Atacamite) and β-$Ni_2(OH)_3Cl$ belong to No. 62 (D_{2h}^{16}), γ-$Cu_2(OH)_3Cl$, and γ-$Cu_2(OD)_3Cl$ belong to No. 14 (C_{2h}^5), β-$Co_2(OH)_3Cl$, β-$Co_2(OH)_3Br$, and β-$Co_2(OD)_3Cl$ belong to No. 166 (D_{3d}^5), the primary cell parameters can be seen in related Refs. [15]–[29].

Figure 1 shows the typical microstructure of a single hydroxyl/deuteroxyl system $M_3 \equiv$OH/D$\cdots X$ with O bridging three metal ions M and H/D bound to a halogen ion by a possible H-bond. From Fig. 1, one can see that the environmental structure of a single hydroxyl system includes two parts, i.e., positive metal ions M (Cu and Co) adjacent to O ion on the O side and negative halogen (Cl and Br) on the H^+ (proton) side, which may possibly be the proton accepter if the H-bond is formed. In order to evaluate the interaction between M and O only from the measured structure parameters, one can simply check the M–O distances $d(MO)$ and compare them with a reference value $d^0(MO)$=$R(M^{2+})$+$R(O^{2-})$, where $R(M^{2+})$ and $R(O^{2-})$ are the common mean ion radius data. If $d(MO) > d^0(MO)$, the interaction may belong to the weak ionic van der Waals type and cause a small effect on the internal OH interaction. When $d(MO) \leq d^0(MO)$, the covalent bond begins to form, and the interaction may belong to the strong covalent type, which can appar-

ently affect the internal OH interaction. The smaller $d(MO)$ is, the weaker the internal OH interaction and the longer d(OH) becomes. This can be understood by the repulsive force along the O–H direction of M^{2+} ion to H^+, or the decrease of O ionic negativity. Here, $R(Cu^{2+})$=0.73 Å, $R(Co^{2+})$=0.745 Å for high spin Co^{2+} (in most of our samples) and $R(O^{2-})$=1.40 Å;[43] therefore, d^0(CuO)=2.13 Å and d^0(CoO)=2.145 Å. One can see that the difference between d^0(CuO) and d^0(CoO) is smaller than 1%.

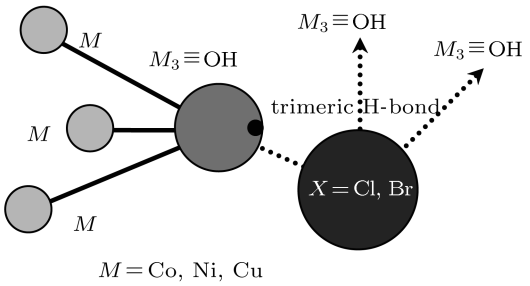


Fig. 1. Typical microstructure of a single $M_3 \equiv$OH$\cdots X$ system with O bridging three metal ions M, H bound to a halogen ion, each M coordinated by other five ligands L_5, and each X bonded probably by the so-called trimeric H-bond.

As to the interaction between M and X, d^0(CuCl) = 2.54 Å, d^0(CuBr) = 2.69 Å, d^0(CoCl) = 2.555 Å, and d^0(CoBr) = 2.705 Å because $R(Cl^-)$= 1.81 Å, $R(Br^-)$ = 1.96 Å, and one can see each X-ion bridges three adjacent M ions besides also bridging three OH groups through the rarely reported possible trimetric H-bond $(OH)_3\cdots X$.[44–47]

Because there may be three different $d(MO)$ for the same bridging O ion, one can estimate reasonably the mean distance according to Coulomb law to be $D(MO)=[3(d_1^{-2}+d_2^{-2}+d_3^{-2})^{-1}]^{1/2}$. Surely for each M ion, the effective charge is smaller than +2 because of the MO_6, MO_5X or MO_4X_2 hexacoordinate structure, and for an M–OH unit, that of the OH group is larger than –1 because of the O bridging structure.

Similarly, a typical H-bond may be formed if the $d(OX)$ is close to the H-bond formation distance $d^0(OX)=R(O^{2-})+R(X^-)$ on the H^+ side and the angle θ(O–H–X) is larger than 120°; therefore, d^0(OCl)= 3.21 Å and d^0(OBr)=3.36 Å.[1–4] Here, the H-bond formation distance can also be described by the $d(H\cdots X)$, but the X-ray diffraction experiments cannot give an exact $d(H\cdots X)$ and the neutron powder-diffraction experiments should use the deuterized sample to measure the $d(D\cdots X)$ to be the $d(H\cdots X)$. The smaller $d(OX)$ is, the stronger the H-bond and the larger d(OH) becomes. This can be understood by the attractive force along the O–H direction of the negative X ion to H^+ and therefore the decreasing O–H force constant.

In fact, according to the different symmetry caused by different d(O–X) of the pyramid $(OH)_3\cdots X$ units, there exist three kinds of trimeric H-bond in the $M_2(OH)_3X$ series: perfect C_{3v} one (in β-$Co_2(OH)_3$Cl/Br), C_s one (in α-$Cu_2(OH)_3$Br, β-$Cu_2(OH)_3$Cl/Br, and β-$Ni_2(OH)_3$Cl), and asymmetric C_1 one (in γ-$Cu_2(OH)_3$Cl).

Now one is aware that the d(OH) is eventually determined by the synergetic effect of M_3 ≡O and possible H-bond $H\cdots X$. Therefore, one can guess that one Raman peak in the functional group (FG) region may be assigned to one ν(OH) corresponding to only one d(OH), and the number of ν(OH) is determined by the number of d(OH) and has no relevance to the number of $d(MO)$ and $d(H\cdots X)$, because the OH stretching vibration frequency (Raman shift) ω_ν(OH) depends on the integrated effect of the whole OH-connecting environment while the number of the OH bending vibration δ(OH), its frequency (Raman shift) is denoted by ω_δ(OH) in the correlation peak (CP) region is not. Therefore, the FG/CP region is just the ν(OH)/δ(OH) region in this paper.

3.2. Determination of hydroxyl vibration regions

The above-mentioned FG and CP regions are generally connected together, although sometimes there are some other vibration modes between them. In order to determine these two regions, besides the empirical estimation, one had better perform the deuterized isotope shift experiments to obtain simultaneously the Raman spectra in FG and CP regions of the OH/D vibration. Figures 2 and 3 show OH/D related parts of the four Raman spectra of γ-$Cu_2(OH)_3$Cl, γ-$Cu_2(OD)_3$Cl, β-$Co_2(OH)_3$Cl, and β-$Co_2(OD)_3$Cl, respectively.

According to the general spectrum analysis method,[48,49] from Fig. 2(a), one can safely assign the Raman peaks (3442/3356/3311) cm^{-1} and (2553/2493/2469) cm^{-1} to ν(OH) and ν(OD) for γ-$Cu_2(OH)_3$Cl and γ-$Cu_2(OD)_3$Cl respectively, and the redshift rates are 74.2%/74.3%/74.6%, which are all close to the estimated rate

$$\sqrt{[16/(1+16)]/[16\times 2/(2+16)]} \approx 72.8\%$$

and correspond to three different d(OH/D) in both samples. From Fig. 2(b), (3559/3546) cm^{-1} and

(2629/2620) cm^{-1} are assigned to ν(OH) and ν(OD) and their Davydov splittings for β-$Co_2(OH)_3Cl$ and β-$Co_2(OD)_3Cl$ respectively, which correspond to one distance d(OH/D) because the neutron diffraction experiments found only one kind of Co_3 $\equiv$OH/D$\cdots$Cl with the d(OH) accuracy of 0.003 Å. Surely they can also be suggested to be two sets of Co_3 $\equiv$OH/D$\cdots$Cl because the splittings are about 10 cm^{-1} and may correspond to a 0.001-Å distance difference according to the famous relation $\Delta\omega_\nu$(OH)=5000 cm^{-1}/Å–12000 cm^{-1}/Å,[11] but this needs more precise neutron diffraction experiments.

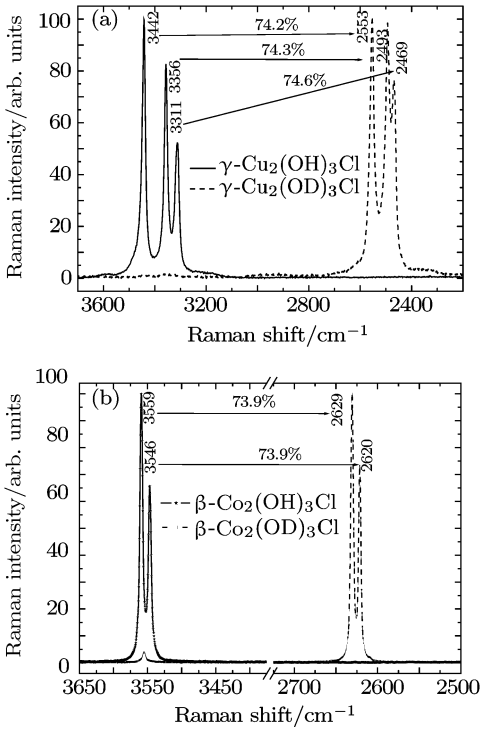


Fig. 2. Raman spectra in the FG region of (a) γ-$Cu_2(OH/D)_3Cl$, and (b) β-$Co_2(OH/D)_3Cl$, respectively.

Similarly, from Fig. 3(a), one can safely assign the Raman peaks (970/927/892/800) cm^{-1} and (726/687/664/587) cm^{-1} to δ(OH) and δ(OD) for γ-$Cu_2(OH)_3Cl$ and γ-$Cu_2(OD)_3Cl$ respectively, and the redshift rates are shown in the figures. Every set of four-peak modes corresponds to nine different CuOH$\cdots$Cl units with the appearance of accident degenerate modes. While figure 3(b) suggests one to safely assign the Raman peaks (828/654) cm^{-1} and (622/478) cm^{-1} to δ(OH) and δ(OD) for β-$Co_2(OH)_3Cl$ and β-$Co_2(OD)_3Cl$ respectively, which correspond to two different CoOH$\cdots$Cl units.

By the way, the peak 3555 cm^{-1} of β-$Co_2(OD)_3Cl$ in Fig. 2(b) and wide 908 cm^{-1} of β-$Co_2(OD)_3Cl$ in Fig. 3(b) may be caused by the small amount of β-$Co_2(OH)_3Cl$ impurity. As to the other peaks in Fig. 3, they are some of the M–O stretching modes not discussed in this paper.

Then, one can confirm that the ν(OH) and δ(OH) regions of our materials are distributed in the ranges of 4000 cm^{-1}–3000 cm^{-1} and 1000 cm^{-1}–600 cm^{-1}, which is very consistent with most of the known experimental facts.[48,49]

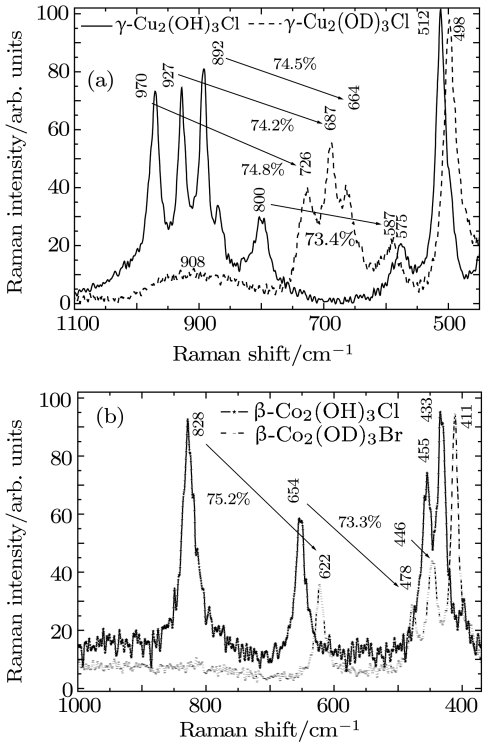


Fig. 3. Raman spectra in the CP region of (a) γ-$Cu_2(OH/D)_3Cl$, and (b) β-$Co_2(OH/D)_3Cl$, respectively.

3.3. Microstructure and Raman ω_ν(OH)

After finding out the ν(OH) and δ(OH) regions, one can continue to check the related Raman data ω_ν(OH)/ω_δ(OH) and the respective crystal structure parameters of those selected samples. Figures 4–6 show the Raman spectra in the FG and CP regions of α-$Cu_2(OH)_3Cl$ and α-$Cu_2(OH)_3Br$, natural β-

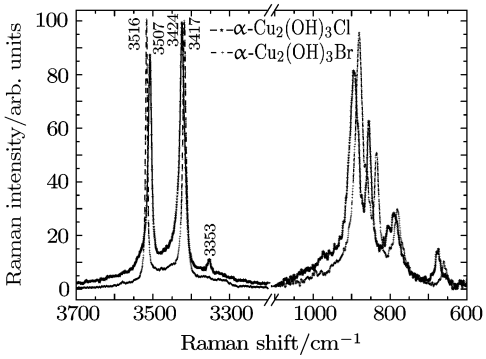


Fig. 4. Raman spectra in the FG and CP regions of α-$Cu_2(OH)_3Cl$ and α-$Cu_2(OH)_3Br$, respectively.

$Cu_2(OH)_3Cl$ and β-$Ni_2(OH)_3Cl$, and β-$Co_2(OH)_3Cl$ and β-$Co_2(OH)_3Br$, respectively (the Raman spectra of γ-$Cu_2(OH)_3Cl$ are shown in Figs. 2(a) and 3(a), and those of β-$Co_2(OH)_3Cl$ are again shown in Fig. 6 to facilitate the comparison with β-$Co_2(OH)_3Br$).

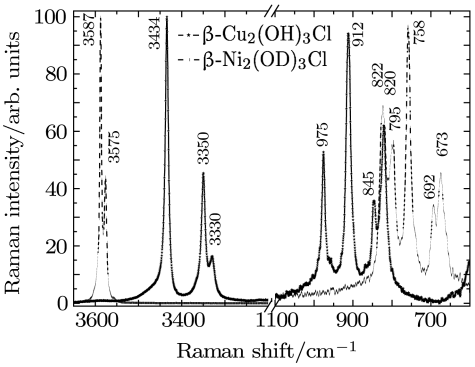


Fig. 5. Raman spectra in FG and CP regions of β-$Cu_2(OH)_3Cl$ and β-$Ni_2(OH)_3Cl$, respectively.

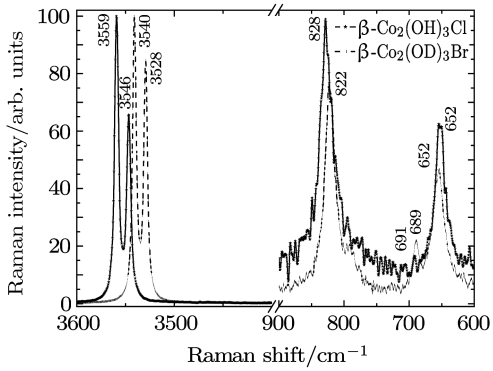


Fig. 6. Raman spectra in FG and CP regions of β-$Co_2(OH)_3Cl$ and β-$Co_2(OH)_3Br$.

The related refined crystal structure parameters, i.e., all the crystallographic distinct distances $d(M_3 \equiv O)/d(OX)/d(OH)$, and Raman shift data belonging to the ν(OH) and δ(OH), are collected in Table 1.

Table 1. Related crystal parameters and Raman shift data in units of Å and cm^{-1}, respectively.

Sample	$d(M_3 \equiv O)$		$D(MO)$	d(OH)	d(OX)	ω_ν(OH)	ω_δ(OH)
α-$Cu_2(OH)_3Cl$	$d(Cu_3 \equiv O^1)$	2.364, 1.936, 1.936	2.052	0.972	3.315	3507	894, 855, 789, 673
	$d(Cu_3 \equiv O^{2,3})$	2.013, 1.974, 2.009	1.999	0.979	3.203	3424	
α-$Cu_2(OH)_3Br$	$d(Cu_3 \equiv O^1)$	2.345, 1.921, 1.921	2.039	0.971	3.525	3516	880, 834, 781, 660
	$d(Cu_3 \equiv O^{2,3})$	2.014, 1.986, 2.038	2.012	0.980	3.310	3418	
β-$Co_2(OH)_3Cl$	$d(Co_3 \equiv O)$	2.079, 2.079, 2.106	2.088	0.966	3.178	3559 3546[c]	828, 652
β-$Co_2(OH)_3Br$	$d(Co_3 \equiv O)$	2.084, 2.084, 2.137	2.101	0.969	3.227	3540 3528[c]	822, 652
Natural β-$Cu_2(OH)_3Cl$	$d(Cu_3 \equiv O^{1,2})$	1.983, 2.018, 2.032	2.011	(0.987)[b]	3.041	3350 3330[d]	975, 912,845, 820, 592[e]
	$d(Cu_3 \equiv O^3)$	1.940, 1.940, 2.412	2.065	(0.978)[b]	3.059	3434	
β-$Ni_2(OH)_3Cl$	$d(Ni_3 \equiv O^{1,2})$	2.062, 2.038, 2.054	2.051	0.952[a] (0.963)[b]	3.186	3587	822, 795, 758, 692, 673
	$d(Ni_3 \equiv O^3)$	2.081, 2.081, 2.090	2.084	0.997[a]	3.134	3575[e]	
γ-$Cu_2(OH)_3Cl$	$d(Cu_3 \equiv O^1)$	2.078, 1.947, 1.991	2.003	1.032[a] (0.991)[b]	3.079	3311	970, 927, 892, 800, 575[e]
	$d(Cu_3 \equiv O^2)$	1.896, 2.382, 1.960	2.049	1.043[a] (0.987)[b]	3.080	3356	
	$d(Cu_3 \equiv O^3)$	2.021, 1.984, 2.047	2.168	0.871[a] (0.977)[b]	2.994	3442	

[a] Value may be doubtful and incorrect.
[b] Value in parentheses is strongly suggested to be confirmed.
[c] Value may be caused by the Davydov splitting effect or by a d(OH) difference of less than 0.002 Å.
[d] Value may be caused by an impurity by a d(OH) difference of less than 0.002 Å.
[e] Value may not be the δ(OH) peak although a large d(CuO)=2.412 Å or 2.382 Å exists in its corresponding material.

From Table 1, one can see that the distinct d(OH) number is at most three in γ-$Cu_2(OH)_3Cl$ because of the Jahn–Teller effect, and the d(OH) of natural β-$Cu_2(OH)_3Cl$ (Atacamite) is now unavailable because these data should be obtained by its deuterized synthetic sample using the neutron powder diffraction

measurement method. Among the ω_ν(OH) values [(3546/3528/3575) cm^{-1}], several are assigned to the small Davydov splittings according to the respective available crystal structures,[50,51] and one (3330 cm^{-1} of β-$Cu_2(OH)_3Cl$) may come from the impurity in the natural sample. Except for the four values, all of the ω_ν(OH) values are definitely assigned to respective crystallographic distinct OH group according to the normal concept that the higher ν(OH) value surely corresponds to the shorter d(OH) regardless of the other part of the hydroxyl system.

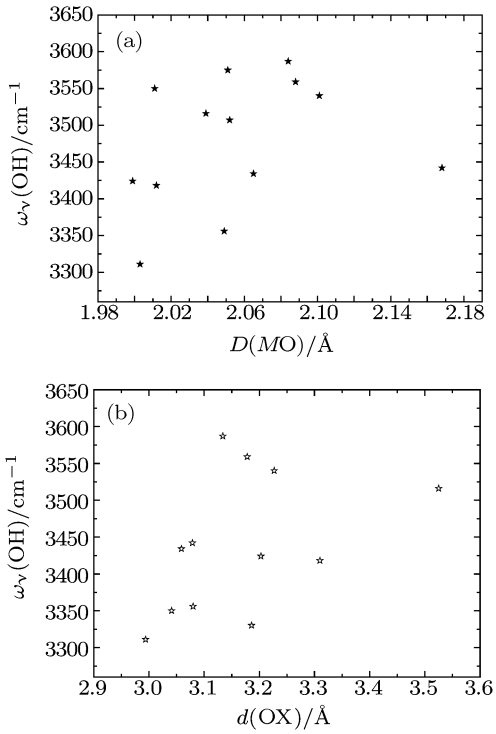


Fig. 7. ω_ν(OH) versus (a) $D(MO)$ and (b) $d(OX)$.

From the detailed $d(M_3 \equiv O)$ and d(OX) data, one can see that most of the MO bonds are strongly covalent for d(CuO) < 2.13 Å or d(CoO) < 2.145 Å and at least one typical H-bond appears in each sample for d(OCl) < 3.21 Å or d(OBr) < 3.36 Å. Therefore, both the M–O bond and the H-bond have exerted an influence on the respective OH group and a distance d(OH) ultimately comes into being to correspond to its ω_ν(OH) value. So the reasonably estimated mean distances $D(MO)$ according to $D(MO)=[3(d_1^{-2}+d_2^{-2}+d_3^{-2})^{-1}]^{1/2}$ are calculated and listed in Table 1 too. Figures 7(a) and 7(b) show ω_ν(OH) versus $D(MO)$ and $d(OX)$ at room temperature, respectively, although it is not strictly reasonable to collect all the data into the same Fig. 7(a) or Fig. 7(b) regardless of the difference between Cu^{2+} and Co^{2+} or Cl^- and Br^-. From Figs. 7(a) and 7(b), one cannot find out any simple correlation between the ν(OH) and $D(MO)$ or $d(OX)$, although it still holds that the shorter $D(MO)$ or $d(OX)$ corresponds to a smaller ω_ν(OH) value when the other conditions do not change.

Like many researchers have done, after ω_ν(OH) versus d(OH) are plotted in Fig. 8, some valuable results can be extracted. Limited by the conditions of the deuterized sample preparation, neutron diffraction measurement and its data analysing experience, the d(OH) values labeled by triangles are doubtful from the beginning. If one accepts that the other experimental data labeled by squares in Fig. 8 are reasonable, an approximately linear relationship between ω_ν(OH) and d(OH) with the change rate $\Delta\omega_\nu$(OH)=–7.26 cm^{-1}/0.001 Å is found in the 270 cm^{-1} difference range of our selected samples, which is consistent with the famous relationship $\Delta\omega_\nu$(OH)=–5000 cm^{-1}/Å–12000 cm^{-1}/Å concluded by Novak.[5]

Till now, one can settle up the following questions:

1) One can guess that there are two distinct d(OH) from the crystal parameters and two different ω_ν(OH), i.e., they may be about 0.978 Å and 0.987 Å respectively, as presented by the black balls in Fig. 8.

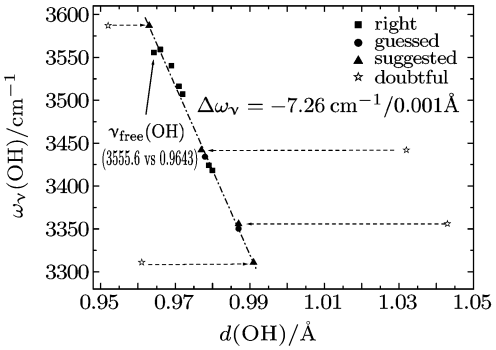


Fig. 8. ω_ν(OH) versus d(O–H). Among the data symbols, squares are the reasonable experimental data except those of a free ν(OH) mode labeled by ν_{free}(OH), stars are the d(OH)-doubtful experimental data, triangles are suggested data to correct the respective star d(OH), and balls are the guessed data whose wavenumber values are from Raman experiments but d(OH) values are unavailable now.

2) Unlike natural β-$Cu_2(OH)_3Cl$ with the same space group of β-$Ni_2(OH)_3Cl$, the latter's ν(OH) has only one value 3587 cm^{-1}, and therefore it has at most two approximately equal d(OH) values even the 3575 cm^{-1} peak is thought to be caused by another different d(OH) value. This can be easily understood by the fact that a short

D(NiO)=2.051 Å with a long d(OX)=3.186 Å and a relatively long D(NiO)=2.084 Å with a relatively short d(OX)=3.134 Å can reasonably give rise to two approximately equal d(OH) values. Therefore, one can correct the two doubtful d(OH)=0.952 Å and 0.997 Å to be 0.963 Å, which needs to be conformed by the future refining experiment, as presented by the triangles at the top of Fig. 8.

3) Similar to 2), one can modify the other three doubtful d(OH)=(1.032/1.043/0.871) Å of γ-$Cu_2(OH)_3Cl$ to be (0.977/0.987/0.991) Å, which are consistent with the exact values (0.962/0.974/0.976) Å given by Wills and Henry using the γ-$Cu_2(OD)_3Cl$ at 2 K.[32]

4) When the well-believed true free OH stretching fundamental frequency $\omega_{\rm free}$(OH) is selected to be 3555.6 cm^{-1} and the bond length d(OH)=0.9643 Å is plotted into Fig. 8,[11] the data point is almost on the fitting line. This firmly verifies the universality of the monotonous change with an approximate linearity.

From the final data group one can estimate that the stretching force constant k(OH) is situated in the range of 6.5 mdyn/Å–7.6 mdyn/Å (1 mdyn=10^{-8} N) for these selected samples.

3.4. Microstructure and Raman ω_δ(OH)

As to the ω_δ(OH) data in the CP region, it is also important to check the more detailed crystal microstructure related to the OH group, because each ω_δ(OH) theoretically corresponds to a special MOH$\cdots X$ with special d(MO), d(OH), d(H$\cdots X$) and the relative space directions (angles). However, from Raman ω_δ(OH) data, one can find that the distinguishable peak number is always less than the number of MOH$\ldots X$ units because the accidental degeneracy usually occurs to result in the additional complexity and difficulty on the exact assignation to a special unit, just like the situation in the fingerprint region. The following points manifest the worthiness of studying the OH related crystal microstructure conformation:

(i) The distinguishable peaks must mean apparently distinct MOH$\cdots X$ units.

(ii) Corresponding to the large ω_ν(OH) value mode with a small interaction between the OH and the adjacent parts, the respective δ(OH) values are usually small, typically like Figs. 4 and 5. This can help to evaluate the interaction strength between the OH and the adjacent parts.

(iii) One can estimate the ratio of ω_δ(OH) to ω_ν(OH) to be about one-fifth to one quarter, and easily find out the range of ω_δ(OH) to justify the OH group and its environment, just as the name of the correlating peak region implies, and subsequently make the peak assignation of the adjacent fingerprint region easier.

4. Conclusion

In conclusion, Raman spectra of 9 kinds of selected basic transition metal halides are measured at room temperature and analysed to investigate their relationship with the microstructured OH environments. Among these selected samples, two deuterized samples are used to determine the ν(OH) region (3600 cm^{-1}–3300 cm^{-1}) and δ(OH) region (1000 cm^{-1}–600 cm^{-1}) of OH systems in the spectra. Through comparative investigation on the distances d(MO), d(OX), and d(OH), the strong M–O interaction and H-bonds are found in each material, but determine simultaneously an ultimate d(OH) and a ω_ν(OH). According to the approximately linear relationship between the ω_ν(OH) and d(OH), to the best of our knowledge, unavailable d(OH) of natural Atacamite (β-$Cu_2(OH)_3Cl$) are guessed and the doubtful d(OH) of γ-$Cu_2(OH)_3Cl$ and β-$Ni_2(OH)_3Cl$ are suggested to be correct. In addition, Raman ω_δ(OH) also manifest their worthiness in research on the OH related crystal microstructure conformation.

In consideration of the complexity of microstructured hydroxyl systems in three-dimensional crystalline solids, each hydroxyl system in a special sample needs further theoretical and experimental studies and optical spectra of other unselected samples of this series should be measured at room temperature and even lower temperatures. Then the above-mentioned states may be greatly improved.

References

[1] Buckingham A D, Del Bene J E and McDowell S A C 2008 *Chem. Phys. Lett.* **463** 1
[2] Arunan E 2007 *Curr. Sci.* **92** 17
[3] Gilli G and Gilli P 2000 *J. Mol. Struc.* **552** 1
[4] Barnes A J 2004 *J. Mol. Struc.* **704** 3
[5] Novak A 1974 *Struc. Bond.* **18** 177
[6] Mikenda W 1986 *J. Mol. Struc.* **147** 1
[7] Beckenkamp K and Lutz H D 1992 *J. Mol. Struc.* **270** 393
[8] Schmidt M and Lutz H D 1993 *Phys. Chem. Minerals* **20** 27

[9] Subramanian S and Zaworotko M J 1994 *Coord. Chem. Rev.* **137** 357

[10] Lutz H D, Mdller H and Schmidt M 1994 *J. Mol. Struc.* **328** 121

[11] Lutz H D 1995 *Struc. Bond.* **82** 85

[12] Libowitzky E 1999 *Monatsh. Chem.* **130** 1047

[13] Mortel R and Lutz H D 2003 *J. Mol. Struc.* **648** 171

[14] Hase Y 2006 *J. Braz. Chem. Soc.* **17** 741

[15] Zheng X G and Otabe E S 2004 *Solid State Commun.* **130** 107

[16] Zheng X G and Xu C N 2004 *Solid State Commun.* **131** 509

[17] Zheng X G, Kawae T, Kashitani Y, Li C S, Tateiwa N, Takeda K, Yamada H, Xu C N and Ren Y 2005 *Phys. Rev.* B **71** 052409

[18] Zheng X G, Mori T, Nishiyama K, Higemoto W, Yamada H, Nishikubo K and Xu C N 2005 *Phys. Rev.* B **71** 174404

[19] Zheng X G, Kubozono H, Nishiyama K, Higemoto W, Kawae T, Koda A and Xu C N 2005 *Phys. Rev. Lett.* **95** 057201

[20] Zheng X G and Nishiyama K 2006 *Physica* B **374–375** 156

[21] Zheng X G, Kawae T, Yamada H, Nishiyama K and Xu C N 2006 *Phys. Rev. Lett.* **97** 247204

[22] Hagihala M, Zheng X G, Toriyi T and Kawae T 2007 *J. Phys.: Condens. Matter* **19** 145281

[23] Zheng X G, Hagihala M, Toriyi T 2007 *J. Magn. Magn. Mater.* **310** 1288

[24] Zheng X G, Hagihala M, Kawae T and Xu C N 2008 *Phys. Rev.* B **77** 024418

[25] Hagihala M, Zheng X G and Kawae T 2009 *Physica* B **404** 671

[26] Fujihala M, Hagihala M, Zheng X G and Kawae T 2009 *Physica* B **404** 674

[27] Zheng X G, Hagihala M, Nishiyama K and Kawae T 2009 *Physica* B **404** 677

[28] Zheng X G, Yamashita T, Hagihala M, Fujihala M and Kawae T 2009 *Physica* B **404** 680

[29] Zheng X G, Hagihala M, Fujihala M and Kawae T 2009 *J. Phys.: Conf. Ser.* **145** 012034

[30] Fujihala M, Hagihala M, Zheng X G and Kawae T 2010 *Phys. Rev.* B **82** 024425

[31] Kim J H, Ji S, Lee S H, Lake B, Yildirim T, Nojiri H, Kikuchi H, Habicht K, Qiu Y and Kiefer K 2008 *Phys. Rev. Lett.* **101** 107201

[32] Wills A S and Henry J Y 2008 *J. Phys.: Condens. Matter* **20** 472206

[33] Wills A S, Perring T G, Raymond S, Fak B, Henry J Y and Telling M 2009 *J. Phys: Conf. Ser.* **145** 012056

[34] Kubo H, Zenmyo K, Tokita M, Hamasaki T, Hagihala M and Zheng X G 2008 *J. Phys. Soc. Jpn.* **77** 013407

[35] Tokita M and Zenmyo K 2009 *J. Phys.: Conf. Ser.* **150** 042208

[36] Maegawa S, Oyamada A, Sato S, Nishiyama M, Itou T and Zheng X G 2009 *J. Phys.: Conf. Ser.* **145** 012018

[37] Maegawa S, Oyamada A and Sato S 2010 *J. Phys. Soc. Jpn.* **79** 011002

[38] Martens W, Frost R L and Williams P A 2003 *N. Jb. Miner. Abh.* **178** 197

[39] Frost R L, Martens W, Kloprogge J T and Williams P A 2003 *J. Raman Spectrosc.* **33** 801

[40] Frost R L 2003 *Spectrochimica Acta* Part A **59** 1195

[41] Macalik L, Maczka M, Solarz P, Fuentes A F, Matsuhira K and Hiroi Z 2009 *Opt. Mater.* **31** 790

[42] Maczka M, Sanjuan M L, Fuentes A F, Macalik L, Hanuza J, Matsuhira K and Hiroi Z 2009 *Phys. Rev.* B **79** 214437

[43] *Ionic Radius Wikipedia, the Free Encyclopedia* http://en.wikipedia.org/wiki/Ionic radius [2011-1-25]

[44] Liu X D**,** Hagihala M, Zheng X G, Tao W J, Meng D D, Zhang S L and Guo Q X 2011 *Chin. Phys. Lett.* **28** 017803

[45] Liu X D, Tao W J, Zheng X G, Hagihala M, Meng D D and Guo Q X 2011 *Acta Phys. Sin.* **60** 037803 (in Chinese)

[46] Liu X D, Hagihala M, Zheng X G and Guo Q X 2011 *Chin. Phys.* B **20** 077801

[47] Liu X D, Hagihala M, Zheng X G and Guo Q X 2011 *Vibrat. Spectrosc.* **56** 177

[48] Nakamoto K 2009 *Infrared and Raman Spectra of Inorganic and Coordination Compounds*, Part A: *Theory and Applications in Inorganic Chemistry* 6th edn. (New York: John Wiley & Sons)

[49] Nakamoto K 2009 *Infrared and Raman Spectra of Inorganic and Coordination Compounds*, Part B: *Applications in Coordination, Organometallic, and Bioinorganic Chemistry* 6th edn. (New York: John Wiley & Sons)

[50] Ergun H B, Gehring K A and Gehring G A 1976 *J. Phys.* C: *Solid State Phys.* **9** 1101

[51] Lagaron J M 2002 *Macromol. Symp.* **184** 19